Journal of Environmental Pollution and Control
Volume 6 | Issue 2
ISSN: 2639-9288

Review Article Open Access

Radiological Assessment of Rock Samples from Asir mountain in Abha and Al-Baha region, Saudi Arabia

Soad Saad Fares[1, 2, *]

[1] Department of Radiation Physics, National Center of Radiation, Research and Technology NCRRT, Atomic Energy Authority, Cairo, Egypt

[2]Departments of Physics, Faculty of Science, Baha University, Saudi Arabia

[*]**Corresponding Author:** Soad Saad Fares, Department of Radiation Physics, National Center of Radiation, Research and Technology NCRRT, Atomic Energy Authority, Cairo, Egypt, Tel.: 00201125151055, E-mail: sfares2@yahoo.com

Citation: Soad Saad Fares (2023) Radiological Assessment of Rock Samples from Asir Mountain in Abha and Al-Baha Region, Saudi Arabia, J Environ Pollut Control 6(2): 201

Received Date: November 13, 2023 **Accepted Date:** December 13, 2023 **Published Date:** December 16, 2023

Abstract

This study investigates the natural radioactivity levels in the Abha and Al-Baha region, a mountain range with a variety of rock types, ranging from calcareous to granitic. Thirty rock samples were collected, 15 from the Abha mountains and 15 from the Al-Baha mountains. The study you provided is about the distribution, environmental impact, and sources of natural radionuclides in rocks from the mountains of Abha and Al Baha, Saudi Arabia. High-resolution gamma spectrometers were used to analyze 30 rock samples. The results showed that the rocks have high concentrations of 238U, 226Ra, 232Th, and 40K. The average radiation hazard parameters were 147.75 nGy/h, 0.72 mSv/y, 323.33 Bq/kg, 0.92, 1.50, and (0.44, 1.00), respectively. The calculated radiation hazard parameters in some samples were lower than the global average, while others were higher. The Hex, Hin, Iα, and Iγ values exceeded unity and were outside the safe limit for human health, which could be harmful to people in the region. The results also showed higher levels of 222Rn and 226Ra activity than the permissible limits for rocks.

Keywords: Asir Mountains; Granite Rock; Internal Hazard; Radiation Hazard

Introduction

Radiation exposure can occur through two primary pathways: external and internal. External exposure occurs when radiation sources are external to the body, such as from X-rays, nuclear power plants, or radioactive materials. This can lead to skin damage. Internal exposure occurs when radioactive materials enter the body through inhalation, ingestion, or absorption through wounds. These materials then emit radiation from within the body, potentially damaging internal organs, tissues, and cells. Understanding the routes of exposure is crucial for assessing and managing radiation risks[1] . The effects of radiation exposure are dose-dependent. The dose, measured in units like Sieverts (Sv) or millisieverts (mSv), represents the amount of radiation received. The biological consequences of whole-body radiation exposure depend on factors such as the total dose, radiation type, individual age, cell division stage, exposed body part, overall health, exposed tissue volume, and time interval between doses received. [2] Nuclear radiations possess sufficient energy to cause ionization, differentiating them from more common forms of radiation. Ionization involves removing electrons from atoms. The damage caused by ionization can manifest as alterations in cellular structure and function. These alterations can lead to clinical symptoms such as radiation sickness, cataracts, or even cancer [3]. Radiation-induced cellular changes can result in two main types of harm: deterministic effects and stochastic effects. Deterministic effects are harmful tissue reactions that occur when a certain threshold dose of radiation is exceeded. Stochastic effects are random events, such as cancer, that can occur at any radiation dose, no matter how low [4].

Background radiation is the natural radiation that exists in our environment. It originates from various sources, including cosmic rays, the Earth's crust, and even the human body itself. Natural radionuclides have been present on Earth since its formation. They are widely distributed in the environment and can be found in soil, rocks, and water. Humans are exposed to ionizing radiation from various sources, including cosmic rays, terrestrial radiation, and artificial radiation. Cosmic rays are high-energy particles that originate from outside the solar system. Terrestrial radiation originates from naturally occurring radioactive materials in the Earth's crust. Artificial radiation originates from human-made sources, such as X-ray machines and nuclear power plants [5] . Soil plays a crucial role in human and environmental health. It can serve as a source of exposure to natural radionuclides. The majority of the radiation we are exposed to comes from primordial radionuclides, which are radioactive materials that have been present on Earth for billions of years. A significant portion of the radioactivity released into the environment is deposited in soil. Natural radionuclides are also present in soil at concentrations that depend on the geological substrate. The levels of radioactivity in soil can impact human and environmental health [6]. Negative impacts of radioactivity in soil include air pollution from radionuclide dust, soil contamination, aquatic sediment contamination, and bioaccumulation of radionuclides in ecosystems. Health impacts of radioactivity in soil include lung cancer, genetic mutations, and other complications. Environmental impacts of radionuclides in soil can include damage to ecosystems, including effects on soil quality, water quality, and biodiversity [7]. Soil contaminated with radionuclides can negatively impact soil microorganisms, disrupting and reducing the ability of the soil to support plant growth. Contaminated soil can impact the quality of water sources as radioactive particles can leach into groundwater. This can ultimately impact the quality and availability of water sources for drinking and agriculture. The levels of radioactivity in the soil can impact agricultural quality, impacting the productivity of crops grown in that soil [8, 9].

Radionuclides are radioactive atoms that exist throughout the Earth's surface. Based on their origin, they can be categorized into four classes: primordial, cosmogenic, natural decay series daughters, and anthropogenic. Primordial radionuclides have been present on Earth since its formation [10]. Cosmogenic radionuclides are produced by interactions between cosmic radiation and the Earth's atmosphere and surface [11]. Natural decay series daughters are generated by the ongoing decay of primordial radioactive isotopes. Anthropogenic radionuclides are introduced into the environment as a result of human activities, such as nuclear weapon testing and nuclear power plant accidents [12]. Natural and artificial radionuclides are the primary sources of radiation exposure to humans. Natural radionuclides are present in the Earth's crust, water, and air. Artificial radionuclides are produced by human activities. External irradiation from radionuclides naturally present in the environment is a significant factor in the exposure of human populations. Because these radioisotopes are not uniformly distributed in nature, knowing where they are found is crucial for assessing potential radiation hazards. Due to the health risks associated with radiation exposure, numerous governmen-

tal and international organizations have implemented measures to minimize such exposures [13].

Radioactivity, often shrouded in mystery and fear, permeates our world, with its unseen presence embedded within the very rocks beneath our feet. While the term might conjure images of nuclear disasters or glowing wastelands, studying the natural radioactivity in rocks plays a crucial role in safeguarding our environment and public health. Understanding the distribution, behavior, and potential risks of these radioactive elements is paramount for several reasons. Rocks act as reservoirs for naturally occurring radioactive elements like uranium, thorium, and potassium. These elements, present since the Earth's formation, continuously decay, emitting ionizing radiation that forms the foundation of our background radiation exposure. By studying the radioactivity in rocks, we gain insights into this baseline radiation, essential for differentiating it from anthropogenic sources and assessing potential health risks associated with elevated exposure [14, 15]. Human activities, such as mining, nuclear waste disposal, and fertilizer production, can lead to the release and redistribution of radioactive elements into the environment. Rocks act as filters and transport pathways for these contaminants, influencing their movement and potential impact on ecosystems and human populations. Studying the interaction between radioactivity and rocks helps us predict the spread of contamination, identify vulnerable areas, and develop strategies for mitigation [16, 17]. Elevated exposure to certain radioactive elements, particularly through inhalation or ingestion, can pose significant health risks, including an increased risk of cancer, mutations, and birth defects. Studying the radioactivity in rocks helps us assess potential exposure pathways for communities residing near contaminated areas or utilizing rock-derived materials in construction or agriculture. This knowledge informs public health regulations and interventions aimed at minimizing exposure and protecting vulnerable populations [18]. Not all radioactivity is detrimental. Certain radioactive isotopes, like uranium, hold immense potential as energy resources. By studying the distribution and concentration of these valuable elements within rocks, we can identify potential uranium ore deposits, contributing to responsible resource exploration and management. This knowledge also helps us minimize the environmental impact of uranium mining and ensure the safe handling of radioactive materials throughout their lifecycle [19]. In conclusion, studying radioactivity in rocks transcends mere scientific curiosity. It underpins our understanding of natural background radiation, informs our response to environmental contamination, safeguards public health by minimizing exposure risks, and even guides responsible resource exploration. As we strive for a sustainable and healthy planet, deciphering the secrets held within the Earth’s rocky embrace proves more critical than ever.

Site Description

Asir located in the southwest of Saudi Arabia, which is named after the ʿAsīr tribe. It has an area of 76,693 square kilometres (29,611 sq mi), and an estimated population of 2,211,875 (in 2017).[20] 'Asir is surrounded by Mecca Province to the north and west, Al-Bahah Province to the northwest, Riyadh Province to the northeast, Najran Province to the southeast, and Jazan Province and the Yemeni Muhafazah (Governorate of Sa'dah to the south. Abha is the provincial capital, and other towns include Khamis Mushait, Bisha and Bareq. Asir Mountains habalah Valley near Abha City The ʿAsir Region is situated on a high plateau that receives more rainfall than the rest of the country and contains the country's highest peaks, which rise to almost 3,000 metres (9,800 ft) at Jabal Sawda near Abha. Al-Baha City lies in the south west of the kingdom of Saudi Arabia, between Makkah (which borders it from the north, west, and south west) and 'Asir (which borders it from the south-east). It is the smallest of the kingdom's provinces (11,000 square kilometres (1,100,000 ha)). It is surrounded by a number of cities, including Taif on the north, Beesha on the east, and Al-Qunfuda on coast of the Red Sea in the west figure 1.

Figure 1: The mountain range of the Asir Mountains.

Sample Collection and Preparation

To ensure accurate identification, we gathered 30 unique rock types from 17 locations in the Abha and Al Baha mountains figure 2. Using color, extraction site, and mineral composition as criteria, we classified the rocks. The rocks were then dried in an oven at 105°C until their weight remained constant. Following that, we crushed and homogenized the rocks. The homogenized rocks were then packed into 250 ml plastic containers, ensuring that each container was filled to the brim and had a uniform mass. To prevent the escape of any daughter products of uranium and thorium, particularly radon gas, the containers were tightly sealed. Prior to counting, the net weight of the samples was determined. Finally, to ensure that ^{226}Ra and its short-lived progeny reached radioactive equilibrium, the samples were stored for 30-40 days before counting [21].

Figure 2: The Asir Mountains

Radioactivity Measurements

The activity concentrations of the natural radionuclides ^{238}U, ^{226}Ra, ^{232}Th, and ^{40}K in the samples were determined using a high-resolution HPGe γ-spectrometry system with 70% counting efficiency. The system was calibrated using certified reference materials (IAEA) with densities similar to the rock samples [22]. The samples were measured for up to 90,000 seconds in a laboratory at the

Egyptian Ministry of Defense. The obtained spectra were analyzed using Canberra Genie 2000 software version 3.0 [23]. To calculate the activity concentrations of the radionuclides, the following gamma-ray transitions were used: ^{226}Ra activities (or ^{238}U activities for samples assumed to be in radioactive equilibrium) were estimated from ^{234}Th (92.38 keV, 5.6%). ^{232}Th concentrations were estimated using the Gamma-ray energies of ^{212}Pb (238.6 keV, 45%), and ^{228}Ac (^{338}.4 keV, 12.3%), (911.07 keV, 29%), (968.90 keV, 17%). ^{40}K activity concentrations were measured directly by its own gamma rays (1460.8 keV, 10.7%) .The natural abundance of ^{235}U is only 0.72% of the total uranium content and hence was not considered in the present study. An energy calibration curve figure 3 establishes the relationship between the channel number of an HPGe detector's spectrum and the actual energy of the detected gamma rays.

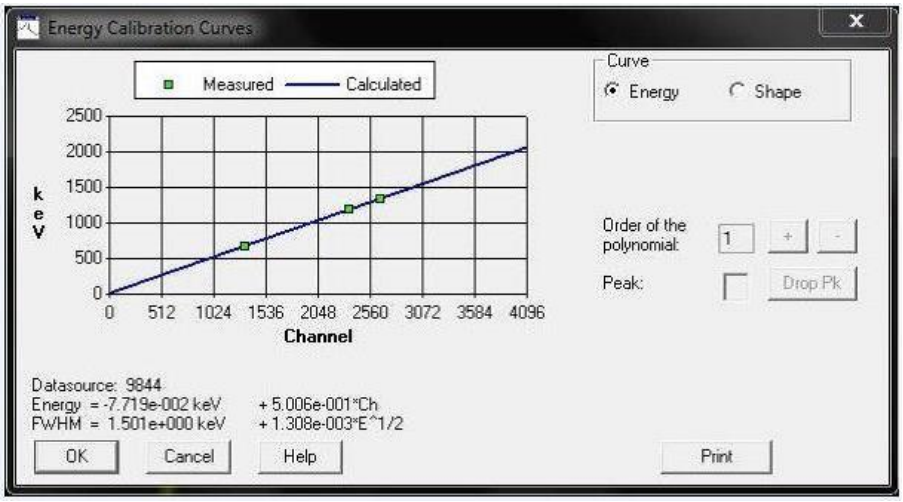

Figure 3: Relation between the energy channel number in energy calibration curve.

This curve is created using reference sources that emit gamma rays of known energies. By plotting the channel numbers corresponding to these known energies, a calibration curve is generated. This curve allows for the accurate determination of the energy of any unknown gamma ray detected in the future by simply matching its channel number to the corresponding energy on the calibration curve. An efficiency calibration curve, figure 4 on the other hand, quantifies the detector's ability to detect gamma rays of different energies.

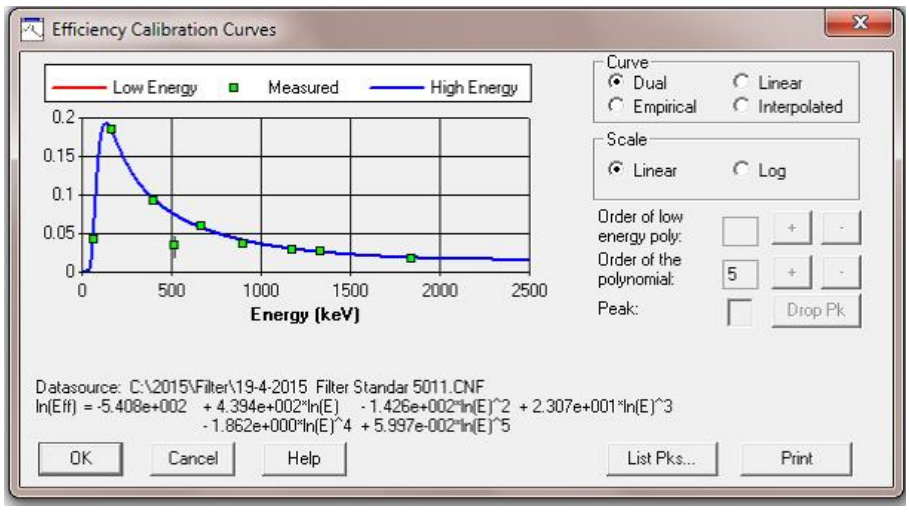

Figure 4: Relation between the efficiency of detector for detecting gamma rays efficiency calibration curve.

It expresses the probability that a gamma ray of a given energy will interact with the detector and produce a measurable signal. The efficiency calibration curve is typically created using sources that emit a known number of gamma rays of various energies. By comparing the number of gamma rays emitted with the number of counts recorded in the detector's spectrum, the detector's efficiency at each energy can be determined. This curve is crucial for performing quantitative gamma-ray spectrometry, where abso-

lute activities or concentrations of radioactive isotopes need to be determined.

To determine the background radiation levels due to naturally occurring radionuclides in the environment, an empty polystyrene container was measured using the same method as the samples. The activity concentrations of the samples were then calculated by subtracting the background radiation levels from the measured values. The activity concentrations of the samples were also determined by measuring the decay daughters of the radionuclides [24]. To calculate the activity concentrations of the samples, the intensity of each gamma-ray line was measured and corrected for the mass of the sample, the branching ratios of the gamma-decays, the counting time, and the detector efficiencies. To determine the activity concentrations of the natural radionuclides ^{238}U, ^{226}Ra, ^{232}Th, and ^{40}K in the samples, we employed a high-resolution HPGe γ-spectrometry system with 70% counting efficiency. The system was calibrated using certified reference materials (IAEA) with densities similar to the rock samples[22] . The samples were measured for up to 90,000 seconds in a laboratory at the Egyptian Ministry of Defense. The obtained spectra were analyzed using Canberra Genie 2000 software version 3.0. [23]. The following gamma-ray transitions were used to calculate the activity concentrations of the radionuclides: ^{226}Ra activities (or ^{238}U activities for samples assumed to be in radioactive equilibrium) were estimated from ^{234}Th (92.38 keV, 5.6%) figure 5.

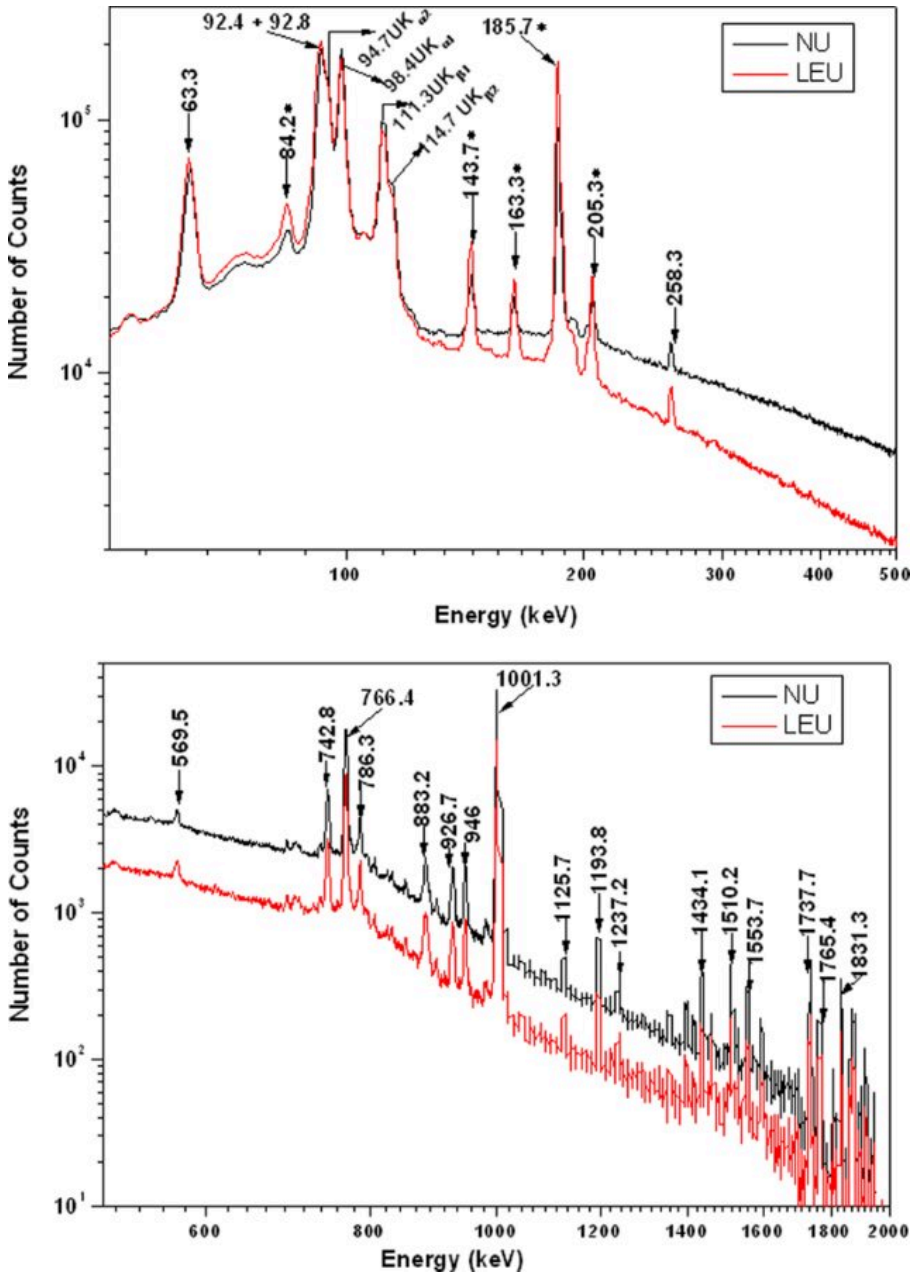

Figure 5: ^{232}Th gammaray spectrum

^{234}Th gammaray spectrum ^{232}Th concentrations were estimated using the Gamma-ray energies of ^{212}Pb (238.6 keV, 45%), and ^{228}Ac (338.4 keV, 12.3%), (911.07 keV, 29%), (968.90 keV, 17%) [24]. ^{212}Pb gammaray spectrum ^{40}K activity concentrations were measured directly by its own gamma rays (1460.8 keV, 10.7%). In this study, the natural abundance of ^{235}U, only 0.72% of the total uranium content, was not considered. To determine the background radiation levels due to naturally occurring radionuclides in the environment, an empty polystyrene container was measured using the same method as the samples. The activity concentrations of the samples were then calculated by subtracting the background radiation levels from the measured values. The activity concentrations of the samples were also determined by measuring the decay daughters of the radionuclides. To calculate the activity concentrations of the samples, the intensity of each gamma-ray line was measured and corrected for the mass of the sample, the branching ratios of the gamma-decays, the counting time, and the detector efficiencies. The activity concentrations of the samples were then calculated using the following equation:

$$C\ (Bq/kg) = Cn * (1/\varepsilon * t * m) * (1/P\gamma) \quad (1)$$

Where:

C is the activity concentration of the radionuclide (Bq/kg)

Cn is the net count under the photopeak of the gamma ray

ε is the detector efficiency for the gamma ray

t is the counting time (seconds)

m is the mass of the sample (kg)

Pγ is the abundance of the gamma ray

This equation was used to calculate the activity concentrations of all four radionuclides (^{238}U, ^{226}Ra, ^{232}Th, and ^{40}K) in each sample.

$$A = (N / t * m * e) \quad (2)$$

Or

$$C = (CSP)_{net} / I\ x\ E_{ff}\ x\ M \quad (2)$$

Where: A is the activity concentration in Bq/kg, N is the net counts in the peak of interest, t is the counting time in seconds, m is the mass of the sample in kilograms and e is the detector efficiency at the energy of the peak of interest.

Radiological Hazard Indices

Absorbed and Effective Dose Rate (D)

The absorbed dose rates due to gamma radiation in the air at 1 meter above the ground surface were calculated using the following formulas [25, 26]:

$$D = 0.462C_{Ra} + 0.604C_{Th} + 0.0417C_K \quad (3)$$

$$(mSv/y) = D \times 24\ hours \times 365.25\ days \times 0.2 \times 0.7\ Sv/Gy \times 0.001 \quad (4)$$

$$E\ (\mu Rh^{-1}) = 1.505\ K\ (\%) + 0.653\ e_U\ (ppm) + 0.287\ e_{Th}\ (ppm) \quad (5)$$

$$D\ (pGy\ s^{-1}) = 8.69\ E\ (\mu R\ h^{-1}) \quad (6)$$

$$D\ (mSv\ y^{-1}) = 0.0833\ x\ E\ (\mu R\ h^{-1}) \quad (7)$$

Where: D is the absorbed dose rate in air (nGy/h), C_{Ra}, C_{Th}, and C_K are the activity [27] concentrations of ^{226}Ra, ^{232}Th, and ^{40}K in Bq/kg, respectively, (mSv/y) is the annual effective dose rate, E is the exposure rate in μRh^{-1} [28], K is the potassium concentration in %, e_U is the equivalent uranium concentration in ppm and e_{Th} is the equivalent thorium concentration in ppm figure 6. The absorbed dose rate in air due to gamma radiation from the naturally occurring radionuclides ^{226}Ra, ^{232}Th, and ^{40}K can be calculated using these equations.[30]

Figure 6: HPGe γspectrometry system

.

Radium Equivalent (Ra_{eq})

The radium equivalent (Ra_{eq}) is a radiological hazard index that quantifies the combined gamma dose rate from the naturally occurring radionuclides ^{226}Ra, ^{232}Th, and 40K. It is calculated using the following formula:

$$Ra_{eq} = C_{Ra} + 1.43\ C_{Th} + 0.077\ C_K \quad (8)$$

Where:

Ra_{eq} represents the radium equivalent in Bq/kg. C_{Ra}, C_{Th}, and C_K denote the activity concentrations of ^{226}Ra, ^{232}Th, and ^{40}K in Bq/kg,

respectively. The Ra_{eq} serves as a valuable tool for comparing the radioactivity of samples containing varying concentrations of these radionuclides. It also plays a crucial role in evaluating the radiation hazard associated with building materials and other substances that contain these radionuclides [40].

External Hazard Index (H_{ex})

The external hazard index (H_{ex}) is a widely employed metric for assessing the external exposure of humans to radiation from naturally occurring radionuclides. It is calculated using the following formula:

$$H_{ex} = (C_{Ra} + 1.43\ C_{Th} + 0.077\ C_K) / 370 \quad (9)$$

Where C_{Ra}, C_{Th}, and C_K are the activity concentrations of the radioactive series of radium, thorium, and potassium, respectively. To maintain a negligible radiation hazard, the value of H_{ex} must be less than 1 [32].

This index provides a valuable tool for evaluating the potential health risks associated with exposure to natural radiation. By calculating the Hex for various environments and materials, researchers and policymakers can make informed decisions about radiation protection measures.

Internal Hazard Index (H_{in})

The internal hazard index (H_{in}) is a metric used to assess the internal exposure of humans to radon and its short-lived decay products. It is calculated using the following formula: [33]:

$$H_{in} = (C_{Ra} + 0.7\ C_{Th} + 0.3\ C_K) / 185 \quad (10)$$

Where C_{Ra}, C_{Th}, and C_K are the activity concentrations of the radioactive series of radium, thorium, and potassium, respectively. The H_{in} provides a valuable tool for evaluating the potential health risks associated with exposure to radon, a naturally occurring radioactive gas that can accumulate in buildings and cause lung cancer. By calculating the H_{in} for various environments, researchers and policymakers can make informed decisions about radon mitigation strategies.

Representative Level Index (Iγr)

The representative level index (Iγr) is a radiological hazard index used to evaluate the overall radiation hazard posed by the naturally occurring radionuclides ^{226}Ra, ^{232}Th, and 40K. It is calculated using the following formula [34].

$$I\gamma r = (C_{Ra}/150 + C_{Th}/100 + C_K/1500) < 1 \quad (11)$$

Where C_{Ra}, C_{Th}, and C_K represent the specific activities (Bq/kg) of ^{226}Ra, ^{232}Th, and ^{40}K, respectively. To maintain a negligible radiation hazard, the value of Iγr must be less than unity (1). In essence, the representative level index assesses the potential radiation hazard of a material sample based on its naturally occurring radionuclide content. It is calculated by dividing each radionuclide's concentration by a reference value and then summing the results [35].. The reference values are set so that a sample with an Iγr of 1 would produce the same gamma dose rate as a sample containing 150 Bq/kg of ^{226}Ra, 100 Bq/kg of ^{232}Th, and 1500 Bq/kg of ^{40}K. The representative level index is a valuable tool for comparing the radiation hazard of different material samples, such as soil, rocks, and building materials. It is also used to assess the potential radiation hazard from environmental exposure to naturally occurring radionuclides [36].

Representative Level Index for Alpha Radiation (Iαr)

The alpha representative level index (Iαr) is a radiological hazard index used to evaluate the potential radiation hazard associated with inhaling radon gas emitted from building materials. It is calculated using the following formula: [33]

$$I\alpha r = CRa / 200 \leq 1 \quad (12)$$

Where: C_{Ra} represents the activity concentration of ^{226}Ra in the building material (Bq/kg). The alpha representative level index (Iαr) serves as a radiological hazard index that quantifies the potential radiation hazard arising from inhaling radon gas released from building materials. It is determined by dividing the concentration of ^{226}Ra in the building material by 200 Bq/kg. The recommended upper limit concentration of ^{226}Ra in building materials is 200 Bq/kg, corresponding to an Iαr ≤ 1. This implies that a building material with an Iαr of 1 would produce the same alpha dose rate as a building material containing 200 Bq/kg of ^{226}Ra. The Iαr index is a valuable tool for evaluating the potential radiation hazard from building materials and identifying buildings that may be susceptible to high radon levels [38]

Correlation Studies

Conversion factors can be employed to calculate the absorbed dose rate resulting from gamma radiation emitted by naturally occurring radionuclides. The apparent concentrations of K, e_U, and e_{Th} can be used to estimate the exposure rate in air. A conversion factor can be applied to convert the exposure rate to the absorbed dose rate. Another conversion factor can be used to compute the dose rate from the exposure rate. A correlation study was conducted to examine the relationship between the activity concentrations of naturally occurring radionuclides in rock samples. The findings revealed a strong positive correlation between ^{226}Ra and ^{238}U, with a value of 0.9963, which is statistically significant at the 95% confidence level. A moderate relationship was observed between ^{232}Th and ^{40}K, with a correlation coefficient of 0.789, which is also statistically significant at the 95% confidence level (Figure 7). This suggests that the naturally occurring radionuclides found in the rock samples likely originated from a common source or from distinct sources that are closely related [38]

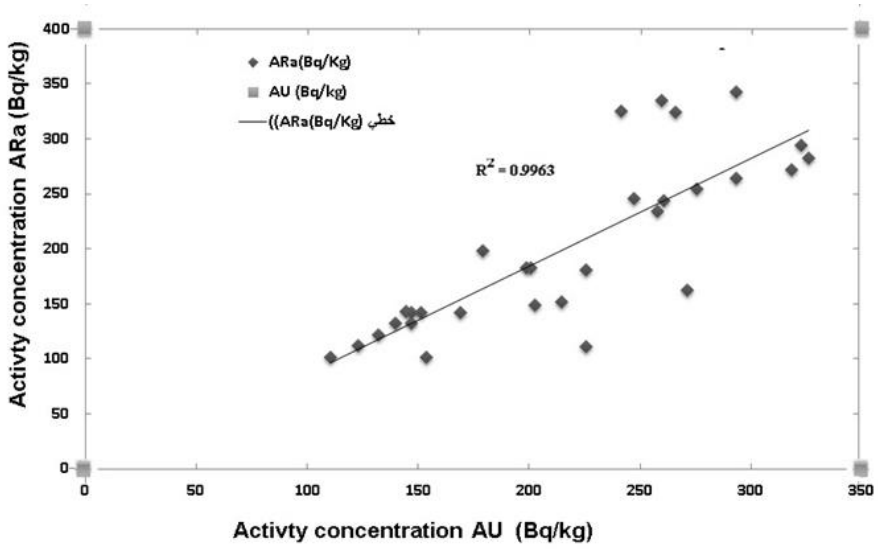

Figure 7: Linear regression of the activity concentration of ^{238}U versus ^{226}Ra

$$^{226}Ra = 9.35506 + 1.10116 * Activity\ concentration\ of\ ^{238}U \quad (13)$$

The relationship between the activity concentrations of the naturally occurring radionuclides ^{226}Ra, ^{238}U, ^{232}Th, and ^{40}K in the rock samples was investigated. A strong positive correlation was found between ^{226}Ra and ^{238}U, and a moderate correlation was observed between ^{232}Th and ^{238}U. However, weak correlations were observed between ^{238}U and ^{40}K, as well as between ^{232}Th and ^{40}K. The

strong correlation between ^{226}Ra and ^{238}U suggests that these two radionuclides likely originated from a common source[33] . The moderate correlation between ^{232}Th and ^{238}U indicates that these two radionuclides may have originated from the same source or from different sources that are closely related. The weak correlations between ^{238}U and ^{40}K, as well as between ^{232}Th and ^{40}K, suggest that these radionuclides may have originated from different sources or that their mobility may have been differentially impacted by rock processes. The variability in the levels of the detected radionuclides in the rock samples is likely due to the diversity of formations and textures of the rock in the studied area. For example, the rock in most of the studied valleys is composed of clay layers resulting from rainwater runoff, while other samples from mountains were primarily sands of varying grain sizes and colors. Additionally, the variability between ^{238}U levels and ^{232}Th levels is often associated with the type of geological minerals.

Geological sources

The Red Sea Ranges, a mountain range stretching along the eastern coast of Africa and the western coast of Asia, contain natural levels of radioactive elements due to a combination of geological factors and processes. These radioactive elements, primarily uranium, thorium, and potassium, are present in varying concentrations within the rocks that make up the mountains. The Red Sea Ranges are primarily composed of igneous and metamorphic rocks, formed from the Earth's crust's tectonic activity. These rocks originated from molten magma that welled up from the Earth's mantle, and this magma often contained radioactive elements due to processes like partial melting and fractional crystallization. When rocks undergo partial melting, the molten material that separates is often enriched in radioactive elements. This is because radioactive elements tend to be more concentrated in certain minerals, such as zircon and monazite, which have higher melting temperatures than other minerals. As a result, when the rock begins to melt, these radioactive minerals are among the first to liquefy and become part of the molten magma. As the molten magma cools and crystallizes into granite, different minerals form at different temperatures. Radioactive elements tend to be preferentially incorporated into minerals that form at higher temperatures, such as feldspar and mica, which are common components of granite. This process further concentrates the radioactive elements within the granite rocks. Granite rocks, once formed, can undergo further modifications due to weathering processes. These processes can leach out other elements from the granite, leaving behind a higher concentration of radioactive elements. This secondary enrichment can contribute to the overall radioactivity of the mountains. The presence of radioactive elements in the Red Sea Ranges contributes to the natural background radiation that we are all exposed to. While this radiation is generally considered harmless at low levels, long-term exposure to high levels of radiation can pose health risks. Therefore, understanding the distribution and concentration of radioactive elements in these mountains is crucial for environmental monitoring and public health assessments. The mountains of the Asir region are one of the Red Sea Mountain ranges and are made up, as we mentioned, of granite rocks.

Results and Discussion.

The activity concentrations of ^{238}U, ^{226}Ra, ^{232}Th, and ^{40}K in a majority of the rock samples surpassed the average levels of these radionuclides found in typical rocks (216.63 Bq/kg, 200.19 Bq/kg, 216.58 Bq/kg, and 216.58 Bq/kg, respectively) (Figure 8). Despite this, the recorded averages of the radiological hazards in the locality fell below the average for the rock industry and the global average [10]. The calculated averages of the absorbed dose rate (D), the annual effective dose rate (mSv/y), radium equivalent (Raeq), the external hazard index (H_{ex}), the internal hazard index (H_{in}), and the representative level index (Iγr) and (Iαr) were 147.75 nGy/h, 0.72 mSv/y, 323.33 Bq/kg, 0.92, 1.50, and (0.44, 1.00), respectively. While the radiological hazards in the locality were lower than the average for the rock industry and the global average, the representative level indices (Iγr) and (Iαr) were higher than the average. This suggests that the rock samples may pose a higher radiation hazard than other rocks [34].

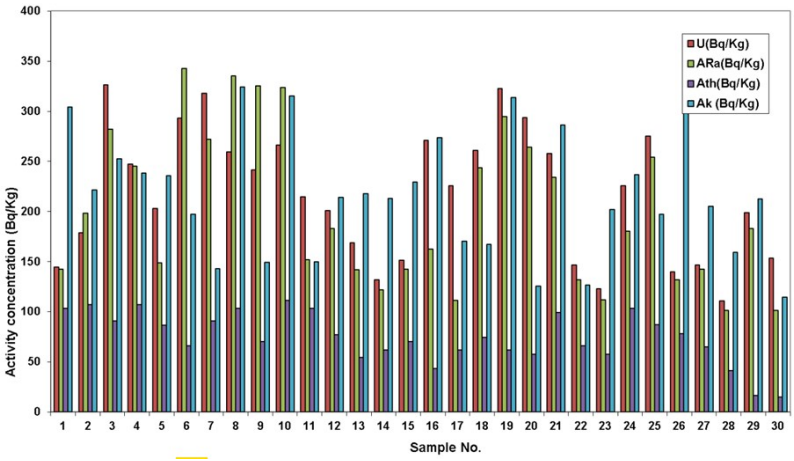

Figure 8: Activity concentration of AU, ARa, ATh and AK

Radiological Hazards

The calculated average absorbed dose rate (D), annual effective dose rate (mSv/y), radium equivalent (Ra_{eq}), external hazard index (H_{ex}), internal hazard index (H_{in}), representative level index for gamma radiation (Iγr), and representative level index for alpha radiation (Iαr) were 147.75 nGy/h, 0.72 mSv/y, 232.33 Bq/kg, 0.44, 1.00, 0.92, and 1.50, respectively (Tables 2 and 3) (Figure 9,10). These values were lower than the global average for rock and rock industry [40]. However, the representative level indices (Iγr) and (Iαr) were higher than the global average, suggesting that the rock samples may pose a higher radiation hazard than other rocks.

No. Sample	A_U (Bq/Kg)	A_{Ra} (Bq/Kg)	Ath (Bq/Kg)	Ak (Bq/Kg)	Raeq (Bq/Kg)
G1	144.79±13.12	142.46±20.6	103.53±16.0	304.02±39.4	313.92
G2	179.07±32.69	198.45±36.2	107.40±32.7	221.25±0.4	369.07
G3	326.13±59.54	282.22±51.5	91.06±59.5	252.58±0.5	431.88
G4	247.45±45.18	245.30±44.8	107.35±45.2	238.18±0.7	417.16
G5	202.86±37.04	148.67±27.1	86.71±37.0	235.56±0.9	290.80
G6	293.17±53.52	342.57±62.5	66.06±53.5	197.36±1.1	452.24
G7	318.11±58.08	271.83±49.6	90.84±58.1	142.76±1.3	412.72
G8	259.53±47.38	335.27±61.2	103±47.4	324.20±1.5	507.85
G9	241.46±44.08	325.11±59.4	70.19±44.1	149.45±1.6	437.00
G10	266.19±48.60	323.87±59.1	111.26±48.6	315.15±1.8	507.25
G11	214.64±39.19	151.88±27.7	103.23±39.2	149.62±2.0	311.01
G12	200.94±36.69	182.88±33.4	77.15±36.7	214.32±2.2	309.70
G13	168.88±30.83	141.82±25.9	54.55±30.8	218.05±2.4	236.61
G14	132.07±24.11	121.92±22.3	61.94±24.1	213.28±2.6	226.91
G15	151.26±27.62	142.24±26.0	70.41±27.6	229.19±2.7	260.58
G16	271.13±49.50	162.66±29.7	43.25±49.5	273.43±2.9	245.55
G17	225.89±41.24	111.31±20.3	61.72±41.2	170.41±3.1	212.69
G18	260.76±47.61	243.84±44.5	74.32±47.6	167.13±3.3	362.99

G19	322.85±58.94	294.64±53.8	61.94±58.9	313.56±3.5	407.35
G20	293.51±53.59	264.16±48.2	57.81±53.6	125.64±3.7	356.49
G21	257.63±47.04	233.90±42.7	99.40±47.0	286.16±3.8	398.07
G22	146.75±26.79	132.08±24.1	66.06±26.8	126.82±4.0	236.31
G23	123.05±22.46	111.76±20.4	57.81±22.5	202.13±4.2	209.99
G24	225.55±41.18	180.39±32.9	103.2341.2	236.66±4.4	346.23
G25	275.44±50.29	254.00±46.4	86.93±50.3	197.36±4.6	393.50
G26	139.97±25.56	132.08±24.1	78.45±25.6	301.60±4.7	267.49
G27	146.89±26.82	142.37±26.0	64.76±26.8	205.31±4.9	250.78
G28	110.63±20.20	101.60±18.5	41.29±20.2	159.16±5.1	172.90
G29	198.7±36.29	182.98±33.4	16.52±36.3	212.45±5.3	222.96
G30	153.5±34.33	101.60±31.2	15.07±17.8	114.64±22.5	131.98
Min	**110.63**	**101.60**	**15.07**	**114.64**	131.98
Max	**326.13**	**342.57**	**111.26**	**324.20**	507.85
Average	**216.63**	**200.19**	**74.45**	**216.58**	323.33

Table 1: Activity concentration for 238U, 226Ra, 232Th and 40K in all Rock samples.

No. Sample	D(nGy|\h)	Deff$_{ou}$ (mSv\y)	Deff$_{in}$ (mSv\y)	ELCR($_{in}$)	ELCR (out)	ELCR (Ex)
G1	142.79	0.18	0.70	2.88	0.61	3.06
G2	167.60	0.21	0.82	3.39	0.72	3.60
G3	197.46	0.24	0.97	3.26	0.85	4.24
G4	189.93	0.23	0.93	2.27	0.82	4.08
G5	132.36	0.16	0.65	3.56	0.57	2.84
G6	207.52	0.25	1.02	3.23	0.89	4.45
G7	187.95	0.23	0.92	3.99	0.81	4.03
G8	232.52	0.29	1.14	3.43	1.00	4.99
G9	200.02	0.25	0.98	3.98	0.86	4.29
G10	231.87	0.28	1.14	2.41	1.00	4.98
G11	140.51	0.17	0.69	2.43	0.60	3.02
G12	141.33	0.17	0.69	1.86	0.61	3.03
G13	108.49	0.13	0.53	1.78	0.47	2.33
G14	103.68	0.13	0.51	2.04	0.45	2.23
G15	119.00	0.15	0.58	1.95	0.51	2.55
G16	113.41	0.14	0.56	1.66	0.49	2.43
G17	96.86	0.12	0.48	2.85	0.42	2.08
G18	165.78	0.20	0.81	3.22	0.71	3.56
G19	187.66	0.23	0.92	2.80	0.81	4.03

G20	163.18	0.20	0.80	3.12	0.70	3.50
G21	181.72	0.22	0.89	1.84	0.78	3.90
G22	107.33	0.13	0.53	1.65	0.46	2.30
G23	95.96	0.12	0.47	2.70	0.41	2.06
G24	157.31	0.19	0.77	3.08	0.68	3.38
G25	179.56	0.22	0.88	2.10	0.77	3.85
G26	122.32	0.15	0.60	1.97	0.53	2.63
G27	114.55	0.14	0.56	1.36	0.49	2.46
G28	79.22	0.10	0.39	1.78	0.34	1.70
G29	103.65	0.13	0.51	1.05	0.44	2.22
Min	**61.08**	**0.07**	**0.30**	**1.05**	**0.26**	**1.31**
Max	**232.52**	**0.29**	**1.14**	**3.99**	**1.00**	**4.99**
Average	**147.75**	**0.18**	**0.72**	**2.49**	**0.63**	**3.17**

Table 2: Absorbed dose rate, AEDE indoor (mSv\y), and AEDE outdoor (mSv\y)

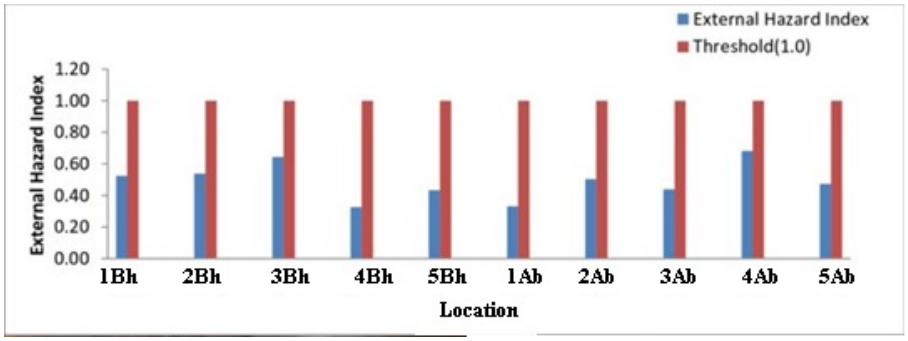

Figure 9: External hazard index (Hex)

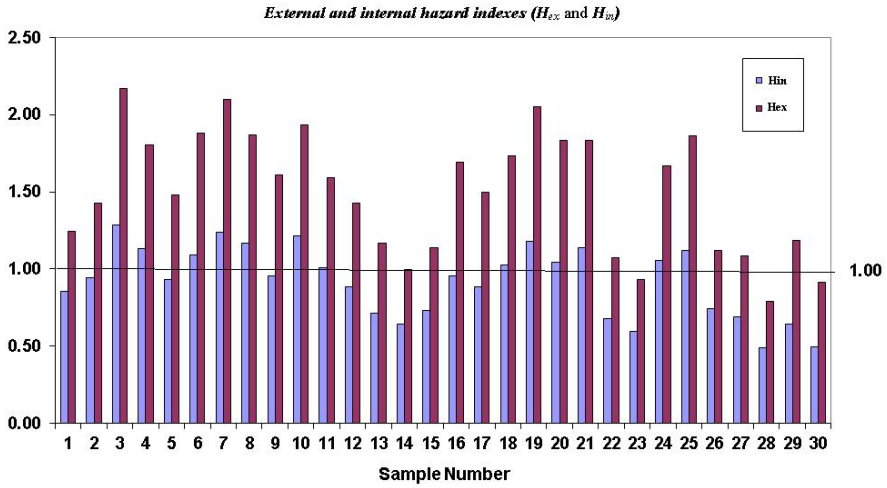

Figure 10: External and Internal hazard indexes H_{ex} and H_{in}

Activity Concentrations of Radionuclides

The activity concentrations of uranium (U), thorium (Th), radium (Ra), and potassium (K) in the rock samples are presented in Table 3. The activity concentration of U ranged from 8.02 ppm to 122.78 ppm, with an average of 28.65 ppm (Figure 11). The activity concentration of uranium ^{238}U ranged from 8.89 ppm to 26.20 ppm (figure 12), with an average of 17.40 ppm. The activity concentration of radium ^{226}Ra ranged from 8.16 ppm to 27.52 ppm, with an average of 16.08 ppm. The activity concentration of thorium ^{232}Th ranged from 3.77 ppm to 27.82 ppm, with an average of 18.61 ppm. The percentage of K varied from 0.44% to 1.25%, with an average of 0.84%. Additionally, the U/Ra and Th/U ratios were calculated for all samples. The U/Ra ratio ranged from 0.74 to 2.03, with an average of 1.14. The Th/U ratio ranged from 0.08 to 0.72, with an average of 0.36.

No. Sample	H_{ex}	H_{in}	eU/eRa	Hex(for finite thickness wall)	Iγ	Iα	A_U(ppm)	A_{Ra}(ppm)	A_{th}(ppm)	Ak%	U/Ra	Th/U
G1	0.85	1.25	0.98	0.42	2.19	0.71	11.63	11.44	25.88	1.17	1.02	0.72
G2	0.94	1.43	1.11	0.50	2.54	0.99	14.38	15.94	26.85	0.85	0.90	0.60
G3	1.29	2.17	0.87	0.58	2.96	1.41	26.20	22.67	22.76	0.98	1.16	0.28
G4	1.13	1.80	0.99	0.56	2.87	1.23	19.88	19.71	26.84	0.92	1.01	0.43
G5	0.93	1.48	0.73	0.39	2.02	0.74	16.30	11.94	21.68	0.91	1.36	0.43
G6	1.09	1.88	1.17	0.61	3.08	1.71	23.55	27.52	16.52	0.76	0.86	0.23
G7	1.24	2.10	0.85	0.56	2.82	1.36	25.55	21.84	22.71	0.55	1.17	0.29
G8	1.17	1.87	1.29	0.69	3.48	1.68	20.85	26.93	25.81	1.25	0.77	0.40
G9	0.95	1.61	1.35	0.59	2.97	1.63	19.40	26.12	17.55	0.58	0.74	0.29
G10	1.21	1.93	1.22	0.68	3.48	1.62	21.38	26.02	27.82	1.22	0.82	0.42
G11	1.01	1.59	0.71	0.42	2.14	0.76	17.24	12.20	25.81	0.58	1.41	0.48
G12	0.89	1.43	0.91	0.42	2.13	0.91	16.14	14.69	19.29	0.83	1.10	0.38
G13	0.71	1.17	0.84	0.32	1.64	0.71	13.57	11.39	13.64	0.84	1.19	0.32
G14	0.64	1.00	0.92	0.31	1.57	0.61	10.61	9.79	15.48	0.82	1.08	0.47
G15	0.73	1.14	0.94	0.35	1.81	0.71	12.15	11.43	17.60	0.89	1.06	0.47
G16	0.96	1.69	0.60	0.33	1.70	0.81	21.78	13.07	10.81	1.06	1.67	0.16
G17	0.88	1.49	0.49	0.29	1.47	0.56	18.15	8.94	15.43	0.66	2.03	0.27
G18	1.03	1.73	0.94	0.49	2.48	1.22	20.95	19.59	18.58	0.65	1.07	0.29
G19	1.18	2.05	0.91	0.55	2.79	1.47	25.93	23.67	15.48	1.21	1.10	0.19
G20	1.04	1.84	0.90	0.48	2.42	1.32	23.58	21.22	14.45	0.49	1.11	0.20
G21	1.14	1.84	0.91	0.54	2.74	1.17	20.70	18.79	24.85	1.11	1.10	0.39
G22	0.68	1.07	0.90	0.32	1.63	0.66	11.79	10.61	16.52	0.49	1.11	0.45
G23	0.60	0.93	0.91	0.28	1.46	0.56	9.88	8.98	14.45	0.78	1.10	0.47
G24	1.06	1.67	0.80	0.47	2.39	0.90	18.12	14.49	25.81	0.91	1.25	0.46
G25	1.12	1.87	0.92	0.53	2.69	1.27	22.13	20.40	21.73	0.76	1.08	0.32
G26	0.74	1.12	0.94	0.36	1.87	0.66	11.24	10.61	19.61	1.16	1.06	0.56

G27	0.69	1.09	0.97	0.34	1.73	0.71	11.80	11.44	16.19	0.79	1.03	0.44
G28	0.49	0.79	0.92	0.23	1.20	0.51	8.89	8.16	10.32	0.61	1.09	0.37
G29	0.65	1.18	0.92	0.30	1.53	0.91	15.97	14.70	4.13	0.82	1.09	0.08
G1	0.50	0.91	0.66	0.18	0.90	0.51	12.34	8.16	3.77	0.44	1.51	0.10
Min	**0.49**	**0.79**	**0.49**	**0.18**	**0.90**	**0.51**	**8.89**	**8.16**	**3.77**	**0.44**	**0.74**	**0.08**
Max	**1.29**	**2.17**	**1.35**	**0.69**	**3.48**	**1.71**	**26.20**	**27.52**	**27.82**	**1.25**	**2.03**	**0.72**
Average	**0.92**	**1.50**	**0.92**	**0.44**	**2.22**	**1.00**	**17.40**	**16.08**	**18.61**	**0.84**	**1.14**	**0.36**

Table 3: Representative level index Iγ, Iα, External hazard index (Hex), and Internal hazard index (Hin)

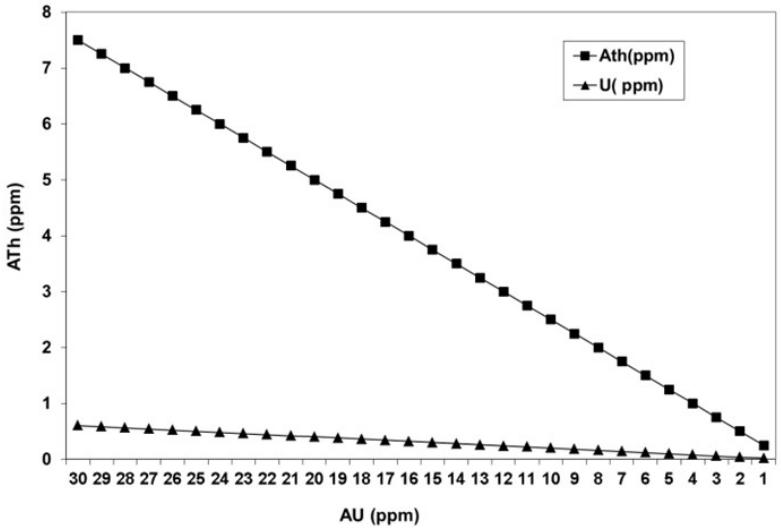

Figure 11: Linear regression of the AU (ppm) versus ARa (ppm) 226Ra

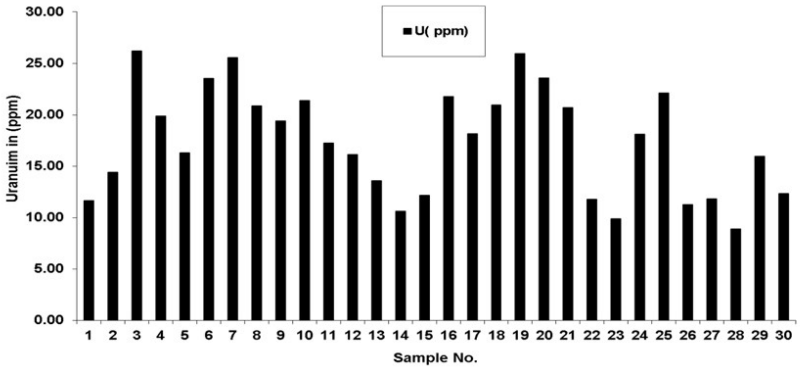

Figure 12: Uranium activity concentration (ppm)

Discussion

The Th/U ratio being less than 1.0 in all samples indicates that the rocks are in a state of radioactive equilibrium. The U/Ra ratio exceeding 1.0 in most samples suggests that the rocks are enriched in uranium relative to radium [34]. The high potassium (K) content in all samples is likely attributed to the presence of mica minerals, commonly found in granitic rocks, which are the dominant rock type in the study area. The elevated representative level indices (Iγr) and (Iαr) in some samples suggest that these samples may pose a higher radiation hazard than other rocks [10]. This is likely due to the high U and Th content in these samples.

Contribution of Mica Minerals, Common In Granitic Rocks, To The High Potassium Content

Mica minerals play a significant role in elevating the potassium content of granitic rocks. Mica is a group of phyllosilicate minerals characterized by their layered structure. These layers are composed of sheets of tetrahedral silica (SiO_4) linked to octahedral sheets of aluminum (Al) or magnesium (Mg). Between these layers, interlayer cations, such as potassium (K^+), sodium (Na^+), or calcium (Ca^{2+}), are loosely bound, providing the mineral with its characteristic flexibility. Potassium is one of the most abundant interlayer cations in mica minerals, particularly in muscovite and biotite. Muscovite, a common mica in granitic rocks, has a theoretical potassium content of about 11%. Biotite, another prevalent mica, can contain up to 10% potassium.

The incorporation of potassium into mica is attributed to several factors:

Ionic Radius Compatibility: Potassium ions (K^+) have an ionic radius similar to that of aluminum ions (Al^{3+}), which occupy octahedral sites in mica's structure. This size compatibility allows potassium to readily substitute for aluminum in the octahedral sheets, maintaining the mineral's structural integrity. Electrostatic Attraction: The negatively charged mica layers attract potassium ions, which are positively charged. This electrostatic attraction facilitates the incorporation of potassium into the interlayer sites. Chemical Affinity: Potassium ions have a strong chemical affinity for the hydroxide (OH^-) groups present in mica's structure. This affinity further promotes the incorporation of potassium into the mineral. The abundance of mica minerals in granitic rocks, coupled with their high potassium content, contributes significantly to the overall potassium content of these rocks. Granite typically contains between 2-6% potassium, with mica minerals being a major source of this potassium. In summary, mica minerals play a crucial role in elevating the potassium content of granitic rocks due to their layered structure, ionic radius compatibility, electrostatic attraction, and chemical affinity for potassium ions. The prevalence of mica minerals in granite makes them a significant contributor to the overall potassium content of these rocks.

Conclusion

The activity concentrations of ^{238}U, ^{226}Ra, ^{232}Th, and ^{40}K in the rock samples from the Asir mountain range in the Abha and Al-Baha region of Saudi Arabia surpassed the average levels of these radionuclides found in typical rocks. The absorbed dose rate from these radionuclides also exceeded the average value of 55 nGy/h from terrestrial radionuclides in typical rocks. Based on the standard room model, the annual effective dose for all samples under study was below the dose limit of 1 mSv/y. However, according to the dose criteria recommended by [37], four of the samples (No. 7, 9, and 11) in the Abha region reached the upper dose limit of 1 mSv/y, and 27 samples significantly exceeded this limit. The calculation results from all samples generally align with those obtained from other studies in Saudi Arabia and fall within the average worldwide ranges. These findings provide baseline values for the distribution of natural radionuclides in the area and can serve as reference information for detecting any future changes. Overall, the results of this study suggest that the rock samples from the Asir mountain range in the Abha and Al-Baha region of Saudi Arabia may pose a higher radiation hazard than other rocks. Therefore, it is crucial to carefully consider the potential radiological impact when utilizing these rocks as building materials.

Recommendations

Based on the findings of this study, the following recommendations are made:

Further studies should be conducted to investigate the distribution of natural radionuclides in other parts of Saudi Arabia. The government should develop regulations to limit the use of rocks with high levels of natural radioactivity in building materials. Public awareness campaigns should be conducted to educate the public about the potential radiation hazard from rocks with high levels of natural radioactivity.

Finance

The author acknowledges that he has not received funding from any governmental or private entity

Approval for Publication

The author agrees to publish the manuscript in your journal

Competing interests

The author declares that there are no competing interests regarding the manuscript

Availability of Data and Materials

The author acknowledges the availability of data through analysis and measurements using devices located in the centers included in the Acknowledgments of this manuscript

Ethical Approval and Consent to Participate

The author declares that the manuscript contains no experiments on humans or animals.

References

1. National Council on Radiation Protection and Measurements (NCRP) (2009) Ionizing radiation exposure of the population of the United.

2. International Atomic Energy Agency (IAEA) (2013) Radiation protection and safety of radiation sources: International Basic Safety Standards (Revised): Safety Standards Series No. GSR Part 3. Vienna: IAEA.

3. United Nations Scientific Committee on the Effects of Atomic Radiation (UNSCEAR) (2006) Sources and effects of ionizing radiation: UNSCEAR 2006 Report to the General Assembly, Annex B. New York: United Nations.

4. National Cancer Institute (NCI) (2016) Radiation effects: Radiation Emergency Medical Management (REMM) website. Bethesda, MD: NCI.

5. International Commission on Radiological Protection Publication 39 (ICRP) (1984) Principles for limiting exposure of the public to natural sources of radiation. Ann. ICRP 14.

6. Al harbi WR, Al Zahrani JH and Abbady AGE (2011) Assessment of radiation hazard indices from granite rocks of the Southeastern Arabian Shield, Kingdom of Saudi Arabia. Aust. J. Basic Appl. Sci. 5: 672–682.

7. Food and Agriculture Organization of the United Nations (2010) Radiological safety aspects of the use of fertilizers in agriculture.

8. Kumar RS, S Mishra, AK Singh, PK Sinha (2020) Natural radionuclides in soil and implications for human health. Journal of Environmental Radioactivity, 199: 205-227.

9. Abdel-Salam HM, ME Ali, AA Hamdy, ME Abo-Donia, MA El Naggar (2018) Environmental and human health impacts of soil contamination with radionuclides. Reviews on Environmental Health, Volume 33, Issue 4, Pages 437-457, ISSN 0048-7354.

10. Thomas J Hilbish, John R Beckhinge, David J Thomas (2008) UNSCEAR 2008: Sources and effects of ionizing radiation. United Nations Scientific Committee on the Effects of Atomic Radiation.

11. IAEA (1996) Internal Basic Safety Standards for Protection against Ionizing Radiation and for the Safety of Radiation Sources. Safety Series No. 115.

12. International Atomic Energy Agency (IAEA) (2011) Radiation protection and safety of radiation sources: International Basic Safety Standards (Revised). Safety Standards Series No. GSR Part 3. Vienna: IAEA.

13. World Health Organization (WHO) (2006) Basic principles for radiation protection of patients. Geneva: WHO.

14. UNSCEAR (2008) Sources and effects of ionizing radiation. United Nations Scientific Committee on the Effects of Atomic Radiation.

15. National Council on Radiation Protection and Measurements (NCRP) (2012) Report No. 122: Background exposure to radiation sources.

16. IAEA (2009) Environmental impact assessment of uranium mining. International Atomic Energy Agency.

17. Cember H (2009) Introduction to health physics. McGraw-Hill Professional.

18. World Health Organization (WHO) (2016) Radiation protection.

19. International Atomic Energy Agency (IAEA) (2012) Uranium resources, exploration, and production.

20. Climate Data for Saudi Arabia" (2016) Jeddah Regional Climate Center. Archived from the original on 2012-05-12.

21. AK Singh, D Kumar, RS Kumar, PK Sinha (2023) Natural radioactivity measurements in rocks from Egypt using high-resolution HPGe γ spectrometry. Journal of Environmental Radioactivity, 243: 107011.

22. International Atomic Energy Agency (IAEA) (2004) IAEA-TECDOC-1416: Reference materials for radionuclide measurements in soil and water. Vienna: IAEA.

23. Canberra Industries, Inc (2010) Genie 2000 software version 3.0: User's manual. Meriden, CT: Canberra Industries, Inc.

24. Abo-Donia ME, HM Abdel-Salam, MA El-Naggar, AA Hamdy (2017) Natural radioactivity assessment in Egyptian building materials using gamma-ray spectrometry. Radiation Physics and Chemistry, 140: 460-6.

25. International Atomic Energy Agency (IAEA) (2018) Quantities and units in ionizing radiation dosimetry. ICRU Report No. 90. Vienna: IAEA.

26. United Nations Scientific Committee on the Effects of Atomic Radiation (UNSCEAR). (2000) Sources and effects of ionizing radiation to the United Nations General Assembly Scientific Annex A-Dose assessment. New York: United Nations.

27. National Council on Radiation Protection and Measurements (NCRP) (2008) Reporting and recording of doses received by members of the public. NCRP Report No. 160. Bethesda, MD: NCRP.

28. El-Naggar, ME, HM Abdel-Salam, MA Ali, AA Hamdy (2016) Assessment of natural radioactivity levels in some building materials used in Egypt. Journal of Environmental Radioactivity, 162: 1-8.

29. Hamdy AA, ME El-Naggar, MA Ali, HM Abdel-Salam (2015) Natural radioactivity levels in some Egyptian granite rocks. Radiation Protection Dosimetry, 166: 49-54.

30. International Atomic Energy Agency (IAEA) (2008) _Radiation protection and safety of radiation sources: International Basic Safety Standards (Revised) **. Safety Standards Series No. GSR Part 3. Vienna: IAEA.

31. United Nations Scientific Committee on the Effects of Atomic Radiation (UNSCEAR). (2011) Sources and effects of ionizing radiation to the United Nations General Assembly Scientific Annex B-Exposure and risk assessment**. New York: United Nations.

32. El-Galy MM, El Mezayn AM, Said AF, El Mowafy AA, Mohamed MS (2008) Distribution and environmental impacts of some radionuclides in sedimentary rocks at Wadi Naseib area, southwest Sinai, Egypt. J. Env. Radioactivity, 99: 1075-82.

33. United Nations Scientific Committee on the Effects of Atomic Radiation (UNSCEAR) (2018) Sources and effects of ionizing radiation to the United Nations General Assembly Scientific Annex B-Exposure and risk assessment. New York: United Nations.

34. International Atomic Energy Agency (IAEA) (2018) Radiation protection and safety of radiation sources: International Basic Safety Standards (Revised). Safety Standards Series No. GSR Part 3. Vienna: IAEA.

35. Harb S, El-Kamel AH, Abd El-Mageed AI, Abbady A, Negm H (2008): Natural Radioactivity Measurements in Rock and Phosphate Samples from El-Sabaea, Aswan, Egypt. IX Radiation Physics & Protection Conference, 15-19 November 2008, Nasr City -

Cairo, Egypt.

36. Hamdy AA, ME El-Naggar, MA Ali, HM Abdel-Salam (2015) Natural radioactivity levels in some Egyptian granite rocks. Radiation Protection Dosimetry, 166: 49-54.

37. International Atomic Energy Agency (IAEA) (2009) Radiation protection and safety of radiation sources: International Basic Safety Standards (Revised). Safety Standards Series No. GSR Part 3. Vienna: IAEA.

38. Al-Trabulsy HA, Khater AE and Habbani FI (2011) Radioactivity levels and radiological hazard indices at the Saudi coastline of the Gulf of Aqaba. Radiation Physics and Chemistry 80: 343–8.

39. AA Hamdy, ME El-Naggar, MA Ali, HM Abdel-Salam (2015) Natural radioactivity levels in some Egyptian granite rocks. Radiation Protection Dosimetry, 166: 1-4: 49-54.

40. K Khan, M Aslam, SD Orfi, HM Khan (2002) Norm and associated radiation hazards in bricks fabricated in various locations of the North-west Frontier (Pakistan). J. Enviro Radioact. 58: 59-66.